Received: 4 March 2025 | Accepted: 3 April 2025

DOI: 10.1002/mgea.70012

RESEARCH ARTICLE

MGE ADVANCES
Materials Genome Engineering

Domain and switching dynamics in antiferroelectric $PbZrO_3$: Machine learning molecular dynamics simulation

Yubai Shi[1,2] | Ruoyu Wang[3,4] | Zhicheng Zhong[3,4] | Yao Wu[5] | Shi Liu[6,7] | Liang Si[8] | Ri He[1,2]

[1]Ningbo Institute of Materials Technology and Engineering, Chinese Academy of Sciences, Ningbo, China

[2]College of Materials Science and Opto-Electronic Technology, University of Chinese Academy of Sciences, Beijing, China

[3]School of Artificial Intelligence and Data Science, University of Science and Technology of China, Hefei, China

[4]Suzhou Institute for Advanced Research, University of Science and Technology of China, Suzhou, China

[5]School of Integrated Circuits, Huazhong University of Science and Technology, Wuhan, China

[6]Department of Physics, School of Science, Westlake University, Hangzhou, China

[7]Institute of Natural Sciences, Westlake Institute for Advanced Study, Hangzhou, China

[8]School of Physics, Northwest University, Xi'an, China

Correspondence

Liang Si and Ri He.
Email: siliang@nwu.edu.cn and heri@nimte.ac.cn

Abstract

Antiferroelectric (AFE) materials have received great attention because of their potential applications in the energy sector. Nevertheless, the properties of AFE materials have not been explored for a long time, especially the atomic-scale understanding of AFE domain walls. Here, using first-principles-based machine learning potentials, we identify the atomic structures, energies, and dynamic properties of the domain walls for AFE lead zirconate. It is found that the domain wall can reduce the critical antiferroelectric-ferroelectric transition field. During the electric field-driven polarization switching process, the domain wall is immobile. Importantly, we observe that a distinct domain structure spontaneously forms in bulk lead zirconate upon annealing at 300 K. The domain structure exhibits an alternating array of clockwise–anticlockwise vortexes along radial with continuous polarization rotation. This anomalous AFE vortex is derived from the energy degeneracy in four possible orientations of the polarization order, which can enhance the dielectric response in the terahertz. The current results give an implication for the emergence of AFE vortex in AFE materials as well as ferroelectric materials.

KEYWORDS

antiferroelectricity, domain wall, machine learning, molecular dynamics

1 | INTRODUCTION

On cooling from paraelectric phases, their ferroelectric (FE) or antiferroelectric (AFE) phases in single crystals can spontaneously form domain structures with different orientations of electric dipoles to minimize the depolarization field energy or elastic energy.[1,2] Domain walls are the boundaries between two adjacent domains that influence the dielectric, ferroelectric, piezoelectric, photovoltaic, and electronic properties of ferric materials. Particularly, domain wall motion driven by an external field is critical for polarization switching, which is characterized by the polarization–electric field (P–E) hysteresis loop of FE and AFE materials.[3] Moreover, the pinning effect of the domain wall from the ionic defects and trapped charges could result in electrical fatigue, which is a major problem hindering the practical applications of FE and AFE. Therefore, an in-depth understanding of the atomistic characteristics of domain walls is crucial for harnessing their distinct properties and enhancing the reliability of FE or AFE electronic devices.[4,5]

Yubai Shi and Ruoyu Wang contributed equally to this study.

In the last decades, the statics and dynamics of FE domain walls have been extensively studied by experiments and theories.[5–8] However, atomic-scale understanding of AFE domains and domain walls is rarely reported because their practical benefits are less accessible than those in FEs.[9] In lead zirconate ($PbZrO_3$, PZO), a representative AFE material, the orthorhombic AFE phase results in 60°, 90°, 120°, and 180° AFE domain walls.[10] High-resolution transmission electron microscope images demonstrate that the electric dipoles in 180° domain walls are parallel, making the walls polar.[11] Compared with 180° domain walls, 90° domain walls are more common in ferroic materials. Most recent experimental and theoretical studies of 90° domain walls have focused on ferroelectric and ferroelastic materials.[12] However, a systematic study of the exact atomic structure details of AFE 90° domain walls is still missing.

Here, we use a machine learning interatomic potential to computationally model the statics and dynamics of PZO and its 90° domain walls, studying their behaviors under an electric field. We identify two types of stable 90° domain wall structures. The domain wall can reduce the critical AFE-FE transition field compared to a single domain. The AFE domain wall is immobile during the electric field-driven polarization switching process, different from domain wall motion in FE. It is also discovered that an AFE vortex structure, which forms spontaneously and exists stably, enhances the dielectric response in both the static and THz frequency ranges. This study provides a deeper understanding of the AFE domain wall and its dynamics at the atomic level, offering opportunities for applications in high-frequency electronic devices.

2 | METHODS

In recent study, we have developed the Deep Potential (DP) model for $PbZr_{1-x}Ti_xO_3$ (PZT) by a machine learning method.[13] It can well reproduce the energy with density functional theory (DFT) level accuracy of PZT in different components. Therefore, the DP model can effectively capture the PZO potential energy surface. For more details on the DFT parameters of the dataset, training parameters, and accuracy test of the DP model, please refer to the Methods section of our recent study.[14,15] For the domain wall structure, due to at least hundreds of atoms are required, which is beyond the capabilities of DFT, there is no domain wall configuration in the training datasets. Nevertheless, the machine learning model can still describe the domain wall structure because the numerous kinds of local atom configurations are explored in training datasets. The distance between domain walls is set to 10 u.c. (~40 Å). Such a long distance is sufficient to prevent coupling between domain walls and to allow the intermediate atoms to converge to the single-domain structure. Based on the DP model and structures of PZO, which contain 40,000 atoms, we conduct molecular dynamics (MD) simulation by using the LAMMPS code with periodic boundary conditions.[16] The temperature range is set from 200 K to 500 K. The simulation environment is set as a triclinic box, allowing for full variation of lattice constants and lattice angles. The time step is set to 0.001 ps, and the equilibrium run is 40 ps. Applying an electric field to the system is achieved by applying an external force to the atoms as an equivalent method. The forces acting on different atoms are determined by multiplying the electric field by the reference Born effective charge. In this study, because of the slight structure distortion of different phases of perovskite, we use the Born effective charge of the cubic structure in all the simulations, whose effective charge tensors are isotropic and diagonal[17]: $Z^*_{Pb} = 3.90$, $Z^*_{Zr} = 5.85$, $Z^*_{O} = -3.25$. The polarization magnitude is calculated by the displacement of all the Pb and Zr atoms relative to their respective oxygen octahedral centers and the corresponding Born effective charges: $\boldsymbol{P} = \sum \left(Z^*_{Pb} \times \boldsymbol{d}_{Pb} + Z^*_{Zr} \times \boldsymbol{d}_{Zr}\right)/V$, where $\boldsymbol{d}$ represents displacement and V the volume of the system. The static dielectric constant is calculated by $\epsilon = \frac{4\pi\beta}{3V}\left[\langle \boldsymbol{P}^2\rangle - \langle \boldsymbol{P}\rangle^2\right] + 1$, where $\beta = 1/k_BT$.[18] $\langle \boldsymbol{P}^2\rangle - \langle \boldsymbol{P}\rangle^2$ is calculated from the polarization values output every 10 steps during an MD simulation of 1,000,000 steps after reaching thermodynamic equilibrium. The frequency-dependent dielectric constant is calculated by $\epsilon(v) = 4\pi\chi(v) + 1$, where v is frequency and χ is the complex electric susceptibility.[19] χ can be obtained using the following equation: $\chi_{\alpha\beta}(v) = \frac{1}{\epsilon_0 V\beta}\left[\langle \boldsymbol{P}_\alpha(t)\boldsymbol{P}_\beta(t)\rangle + i2\pi v \int_0^\infty dt e^{i2\pi vt}\langle \boldsymbol{P}_\alpha(t)\boldsymbol{P}_\beta(0)\rangle\right]$, where α and β define Cartesian components, ϵ_0 is the dielectric constant in vacuum, and $\boldsymbol{P}(t)$ is the electric dipole moment of the system at time t.

3 | RESULTS AND DISCUSSIONS

We start with the crystal structure of bulk PZO. At high temperatures, PZO exhibits a paraelectric cubic phase. It experiences a phase transition from the paraelectric phase to the ground state of the AFE orthorhombic phase (*Pbam*) below ~500 K in the experiment. The AFE phase possesses the alternating positive and negative polarization arrangement along [110], which is primarily contributed by the displacement of the Pb atoms. Nevertheless, it is found that another AFE *Pnam* phase has lower energy than that of the *Pbam* phase. Unlike the *Pbam* AFE phase, in the *Pnam* phase, the Pb atoms exhibit a local displacement component along the [001] direction, alternating between positive, zero, and negative displacements as shown in the inset of Figure 1. The *Pnam* phase has an additional staggered oxygen octahedron rotation around the [001] axis. Thus, the periodicity of four layers along the [001] direction in the structure results in the 80-atom primitive cell of the *Pnam* phase. Our calculations show that the energy of the *Pnam* phase is 0.28 meV/atom lower than that of the *Pbam* phase. The calculated energy landscape from the *Pnam* to the *Pbam* phase illustrates that the *Pbam* phase is located at the maximum of the energy landscape, demonstrating the

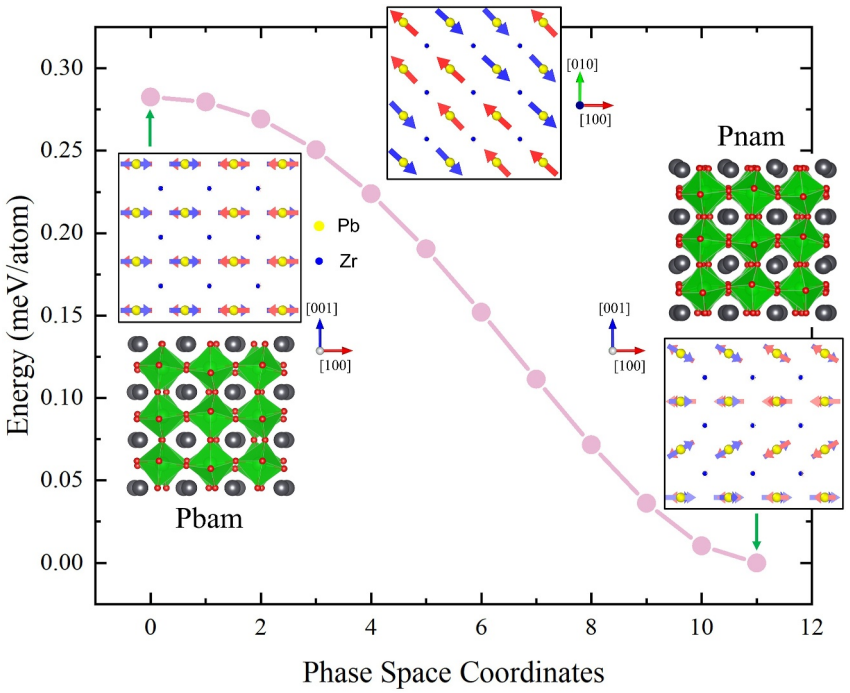

FIGURE 1 The energy landscape as a function of switching pathway from Pbam to Pnam structure.

unstable structure of the *Pbam* phase. This result agrees well with the imaginary frequency of the *Pbam* phase in the recent phonon spectrum calculation.[20]

Next, we investigate the polarization dynamics of PZO. We calculate the polarization response of PZO to the external electric field along [111] at finite temperatures. According to the phase diagram of PZO in our recent study, the DP-predicted AFE-PE transition temperature is 460 K,[14] slightly underestimated compared to the experimental value. Therefore, at 500 K, the MD-calculated P–E loop exhibits a paraelectric linear relationship (Figure 2a). When cooling down to 450 K, PZO begins to exhibit the typical double hysteresis P–E loop in Figure 2a. As the temperature further decreases to 425 K, the double hysteresis loop expands, indicating the higher energy cost during the AFE-FE phase transition. To clarify polarization switching dynamics from the atomic scale, we present the snapshots of the dipole configurations in the (001) plane at several stages on the hysteresis P–E loop at 425 K (see Figure 2b–g). As the electric field is applied, the energies of dipoles with ↑ and ↓ polarization are not equal. At E = 110 kV/cm, AFE order ↑↑↓↓ is destroyed, becoming the ↑↑↑↓↓ order. When E increases to 130 kV/cm, the PZO becomes the FE *R*3*c* phase. Upon the removal of the electric field, the dipole configuration recovers to the AFE order with zero polarization. It should be noted that the FE *R*3*c* phase is metastable, which means that it can be stable at low temperatures. Our MD simulation also shows that the *R*3*c* phase cannot recover to the AFE order, maintaining a large polarization below 200 K.

The above results illustrate that the critical electric field of the AFE-FE phase transition is related to the thermodynamic stability of the AFE phase. Therefore, we investigate the relationship between the critical electric field and temperature. The P–E curves from 200 K to 450 K are calculated by MD simulations (see Figure 3a). The polarization jumps as the electric field increases to the critical value, indicating that the AFE-FE phase transition occurs. The critical electric field decreases as the temperature increases. For instance, the critical electric field is 840 kV/cm at 200 K, whereas it decreases by one order of magnitude at 450 K. We plot the critical electric field versus temperature in Figure 3b, and it exhibits a linear relationship. The simulated critical electric field results are overestimated compared to experimental values.[21] We attribute this discrepancy to the multidomain and polycrystalline nature of experimental samples, whereas our result is based on single-domain systems.

Domain walls play a crucial role in the FE switching dynamics and have been extensively studied.[8,22,23] However, the understanding of AFE domain wall properties at the atomic level remains limited. Here, we focus on the 90° domain wall structure in AFE-PZO. Three geometrically possible configurations are constructed according to the arrangement of dipoles at domain walls: head-to-head (HH), head-to-tail (HT), and alternate types, as shown in Figure 4a–c. The DP model for the structural relaxation leads to the optimized supercells with various domain walls. It is found that HH is unstable, which converts to HT through shifting the domain wall by one unit cell. HT and alternate domain walls are stable after structural relaxation. The

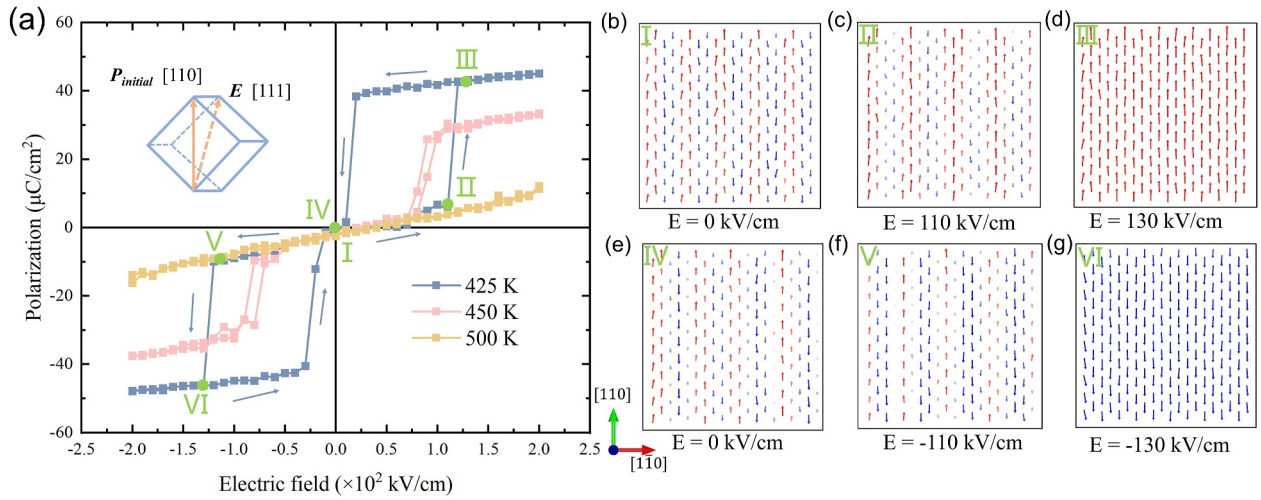

FIGURE 2 (a) Polarization hysteresis loop of PZO at 425 K, 450 K, and 500 K. The initial polarization orientation is along [110], and the electric field orientation is along [111]. Polarization magnitude is projected to [111]. (b)–(g) Snapshots of dipole configurations under different electric fields in the polarization hysteresis loop at 425 K.

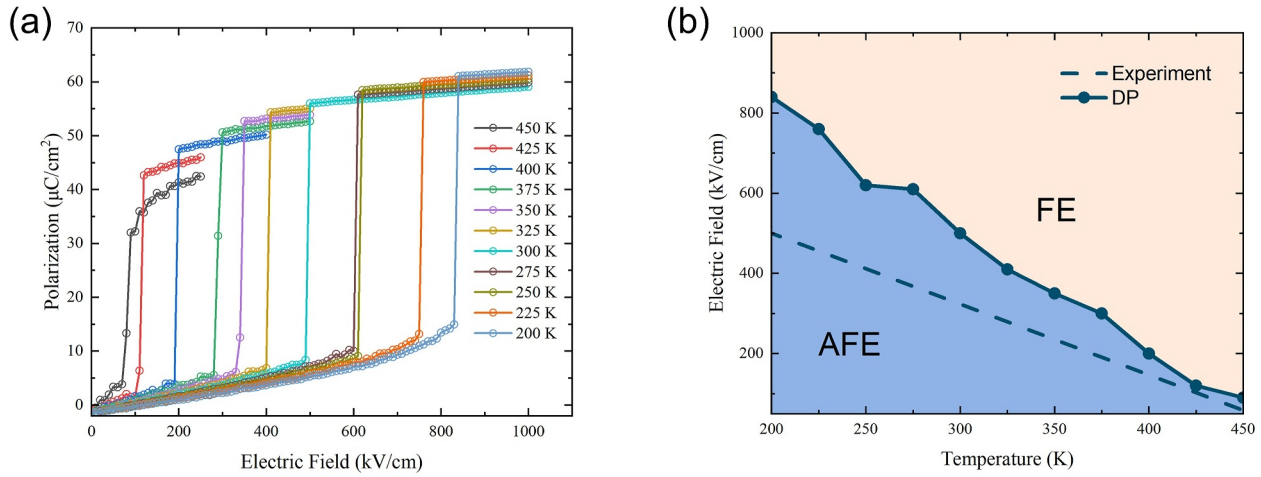

FIGURE 3 (a) Polarization–electric field curve of PZO at different temperatures. (b) The electric field–temperature phase diagram of PZO. The solid line represents the DP-predicted results, and the dashed line represents the experimental results.

domain wall energies of HT and alternate types are 47.52 mJ/m^2 and 43.22 mJ/m^2, respectively, indicating that the alternate type is the most stable. The atom structures of the stable HT and alternate types of 90° domain wall are shown in Figure 4d–g. The alternate-type domain wall is transformed from a line to an armchair shape, in which the HH arrangement disappears, leaving only head-to-tail and tail-to-tail arrangements. It is worth noting that Pb atom displacements along [001] are staggered on either side of the domain wall.

The domain wall dynamics under an electric field are crucial for understanding the polarization switching of AFE. We next study the dynamics of these two types of 180° domain wall structures under an electric field at room temperature. It is found that the existence of a domain wall can reduce the critical electric field, and the AFE domain wall is pinned under an electric field, unlike the FE domain wall. As shown in Figure 5a,b, the AFE-FE phase transition of a single domain is regular and the critical electric field is 500 kV/cm, whereas PZO with domain walls can reduce the critical electric field to 400 kV/cm. When a 400 kV/cm electric field is applied, the AFE domains collinear with the electric field direction first transform into FE domains, and then the remaining dipoles directly reorient toward the field direction. This demonstrates that the switching dynamics of AFE multidomain structures under an electric field differ from those of FE multidomain, which is mediated by domain wall motion. It is also worth noting that the behavior of the 180° domain wall is different from that of the 90° one. Dipole orders ↑↑↓↑↑, ↑↑↓↓↓↑↑, and ↑↑↓↓↓↓↑↑ are 180° domain walls.[20,24,25] They can form and dissipate in the field-driven AFE-FE phase transition process (see Figures 2 and 5).

PZO with an unstable domain wall can transform into an unconventional domain structure under thermal

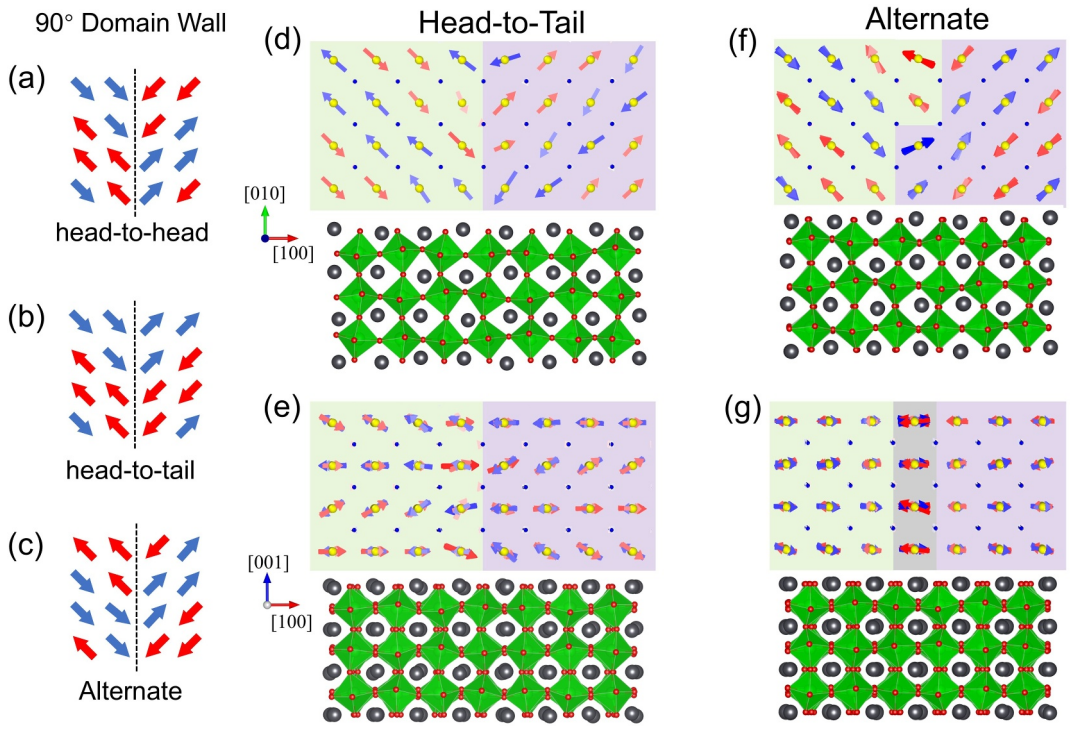

FIGURE 4 The dipole configurations and atomic structures of different 90° domain walls.

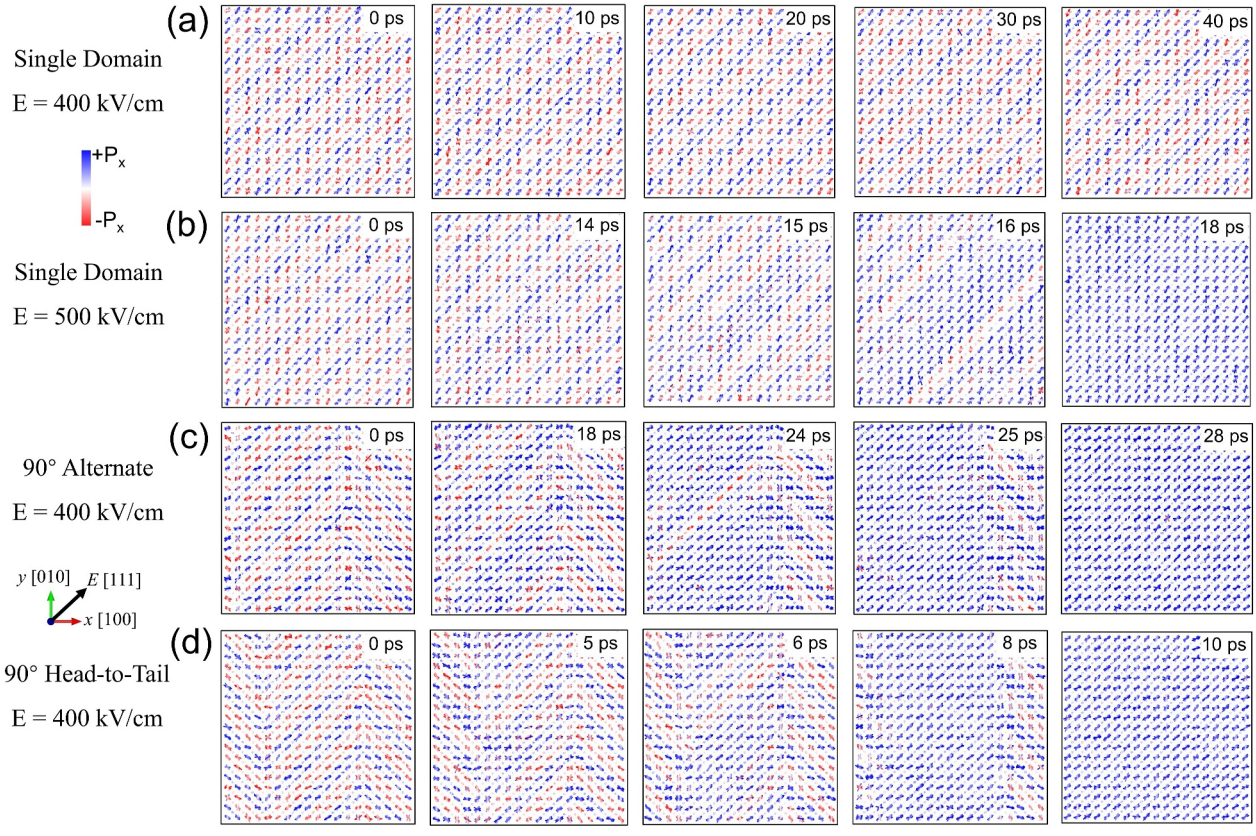

FIGURE 5 The dipole configuration evolution of PZO under an electric field of (a) and (b) single domain, (c) 90° alternate domain wall, and (d) 90° head-to-tail domain wall at 300 K, respectively.

fluctuation. The structure with the HH domain wall can form an AFE vortex structure spontaneously and remain stable under thermal fluctuations when it anneals at 300 K (see Figure 6). Such a vortex is composed of four single domains, divided by alternate and HT domain walls in a cross shape. The dipole orientations of the four domains follow clockwise and counterclockwise interlocked configurations. We predict that in the experiment, annealing from the unstable paraelectric phase at the high temperature (higher than the antiferroelectric-paraelectric transition temperature) can lead to a multidomain structure. It could possibly form the domain wall crossing, inducing the AFE vortex, which can be observed by TEM and SEM in the experiment.

This AFE vortex exhibits dielectric properties distinct from those of the single domain. We calculate the static relative dielectric constant of the single domain, domain wall in the alternate type, and vortex structure for comparison. As shown in Table 1, the vortex structure can significantly enhance the dielectric response in all three directions, with the largest enhancement observed in the z direction. The frequency-dependent dielectric constant is also calculated (see Figure 7). In the THz frequency range of the electric field, the real part of the dielectric constant of the vortex

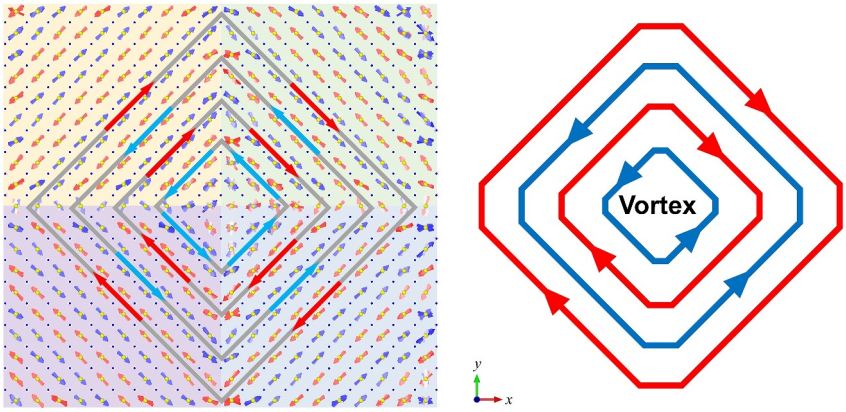

FIGURE 6 A special vortex dipole configuration of PZO, composed of four single domains. The dipoles are alternately arranged in clockwise and counterclockwise rotations.

TABLE 1 Static relative dielectric constant ϵ of different domain structures of PZO.

Domain structure	x component	y component	z component
Single domain	125.93	124.12	234.76
Domain wall	152.82	147.64	306.97
Vortex	202.87	222.56	370.15

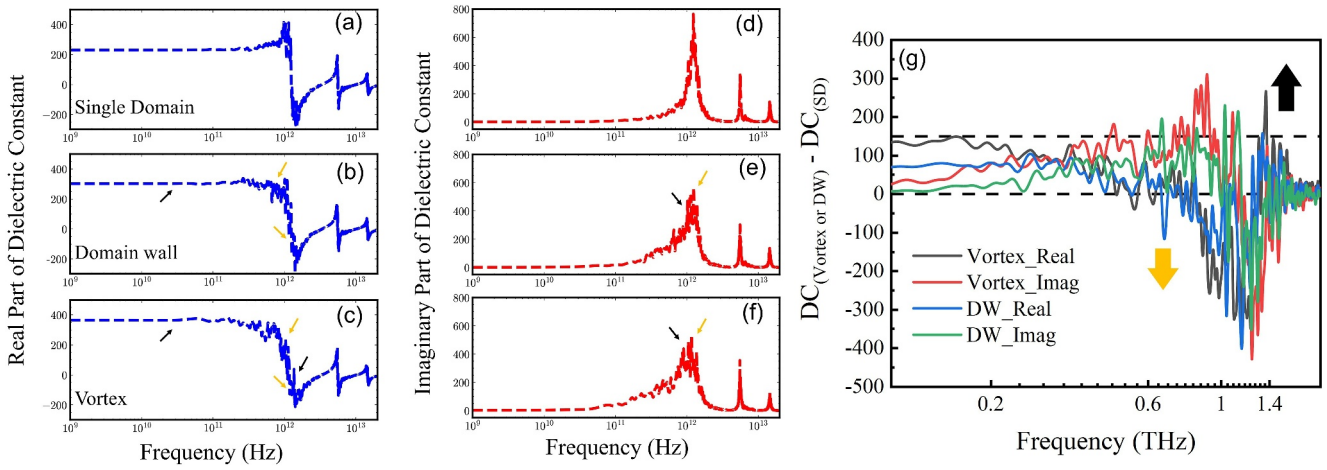

FIGURE 7 The frequency-dependent relative dielectric constant in the z direction of PZO with different domain structures—single domain (SD), domain wall (DW), and vortex. (a)–(c) show the real part and (d)–(f) show the imaginary part. (g) The dielectric constant in the THz frequency range. It shows the differences between domain wall, vortex structure, and single domain, respectively. The yellow arrows indicate a decrease in the dielectric constant, whereas the black arrows indicate an increase, compared to the single domain structure.

structure displays a trend of first decreasing and then increasing. The imaginary part exhibits the opposite trend. Around 1.4 THz, the real part of the dielectric constant of the vortex structure is greater than that of the single domain, whereas the imaginary part is smaller than that of the single domain. This indicates a stronger polarization response capability and lower energy dissipation.

4 | CONCLUSION

In summary, by applying machine learning interatomic potential-assisted MD simulations, we discuss the polarization switching dynamics of PZO at different temperatures and the variation in the critical electric field. We investigate the static properties of the 90° domain wall in AFE-PZO and identify two types of stable domain wall structures, with the alternate type being the most energy favorable domain wall type. It is found that the 90° domain wall in PZO is pinned under an electric field, with the dipoles in each domain reorienting individually. This contrasts with the polarization switching in FEs, which is driven by domain wall motion. We also discover a spontaneously formed and stably existing AFE vortex structure at room temperature, which can enhance the dielectric response and decrease the dielectric loss under a THz electric field. This study provides deep insights into AFE switching dynamics and offers potential for the application of AFE in high-frequency electronic devices.

AUTHOR CONTRIBUTIONS

Ri He and Liang Si conceived the project and supervised the research. Yubai Shi and Ruoyu Wang did investigation and theoretical formal analysis. Yao Wu and Shi Liu provided assistance in formal analysis. Ri He, Liang Si, and Zhicheng Zhong provided funding support. Yubai Shi organized and wrote the paper. Ri He helped to revise the paper and provided scientific discussion when this study encountered problems.

ACKNOWLEDGMENTS

This study was supported by the National Natural Science Foundation of China (Grant Nos. 92477114, 12204496, and 12422407), the Zhejiang Provincial Natural Science Foundation (Grant No. Q23A040003), and the Ningbo Natural Science Foundation (No. 2023J360).

CONFLICT OF INTEREST STATEMENT

The authors declare no conflicts of interest.

DATA AVAILABILITY STATEMENT

The data that support the findings of this study are available from the corresponding author upon reasonable request.

ORCID

Yubai Shi https://orcid.org/0009-0002-7381-3769
Zhicheng Zhong https://orcid.org/0000-0002-7696-934X
Liang Si https://orcid.org/0000-0003-4709-6882

REFERENCES

1. Očenášek J, Minár J, Alcalá J. Dynamics of lattice disorder in perovskite materials, polarization nanoclusters and ferroelectric domain wall structures. *npj Comput Mater*. 2023;9(1):118.
2. Nataf G, Guennou M, Gregg J, et al. Domain-wall engineering and topological defects in ferroelectric and ferroelastic materials. *Nat Rev Phys*. 2020;2(11):634-648.
3. McGilly L, Yudin P, Feigl L, Tagantsev A, Setter N. Controlling domain wall motion in ferroelectric thin films. *Nat Nanotechnol*. 2015;10(2):145-150.
4. Liu S, Grinberg I, Rappe AM. Exploration of the intrinsic inertial response of ferroelectric domain walls via molecular dynamics simulations. *Appl Phys Lett*. 2013;103(23):232907.
5. Liu S, Cohen R. Origin of stationary domain wall enhanced ferroelectric susceptibility. *Phys Rev B*. 2017;95(9):094102.
6. Zhang X, Wang B, Ji Y, et al. First-principles calculations of domain wall energies of prototypical ferroelectric perovskites. *Acta Mater*. 2023;242:118351.
7. Yang T, Wang B, Hu J-M, Chen L-Q. Domain dynamics under ultrafast electric-field pulses. *Phys Rev Lett*. 2020;124(10):107601.
8. He R, Wang H, Liu F, Liu S, Liu H, Zhong Z. Unconventional ferroelectric domain switching dynamics in $CuInP_2S_6$ from first principles. *Phys Rev B*. 2023;108(2):024305.
9. Si Y, Zhang T, Liu C, et al. Antiferroelectric oxide thin-films: fundamentals, properties, and applications. *Prog Mater Sci*. 2024;142:101231.
10. Tanaka M, Saito R, Tsuzuki K. Electron microscopic studies on domain structure of PbZrO3. *Jpn J Appl Phys*. 1982;21(2R):291.
11. Liu Y, Niu R, Majchrowski A, et al. Translational boundaries as incipient ferrielectric domains in antiferroelectric PbZrO 3. *Phys Rev Lett*. 2023;130(21):216801.
12. Liu S, Grinberg I, Rappe AM. Intrinsic ferroelectric switching from first principles. *Nature*. 2016;534(7607):360-363.
13. Zhang L, Han J, Wang H, Car R, E W. Deep potential molecular dynamics: a scalable model with the accuracy of quantum mechanics. *Phys Rev Lett*. 2018;120(14):143001.
14. Shi Y, He R, Zhang B, Zhong Z. Revisiting the phase diagram and piezoelectricity of lead zirconate titanate from first principles. *Phys Rev B*. 2024;109(17):174104.
15. Shi Y, Shan Y, Wu H, Zhong Z, Li R-W, He R. Compositional ordering driven morphotropic phase boundary in ferroelectric solid solutions. *Phys Rev B*. 2024;110(5):054102.
16. Wang H, Zhang L, Han J, Weinan E. DeePMD-kit: a deep learning package for many-body potential energy representation and molecular dynamics. *Comput Phys Commun*. 2018;228:178-184.
17. Zhong W, King-Smith R, Vanderbilt D. Giant LO-TO splittings in perovskite ferroelectrics. *Phys Rev Lett*. 1994;72(22):3618-3621.
18. Caillol J, Levesque D, Weis J. Theoretical calculation of ionic solution properties. *J Chem Phys*. 1986;85(11):6645-6657.
19. Wang D, Hlinka J, Bokov A, et al. Fano resonance and dipolar relaxation in lead-free relaxors. *Nat Commun*. 2014;5(1):5100.
20. Zhang H, Thong H-C, Bastogne L, Gui C, He X, Ghosez P. Finite-temperature properties of the antiferroelectric perovskite PbZrO 3 from a deep-learning interatomic potential. *Phys Rev B*. 2024;110(5):054109.

21. Fesenko O, Kolesova R, Sindeyev YG. The structural phase transitions in lead zirconate in super-high electric fields. *Ferroelectrics*. 1978;20(1):177-178.
22. Bian R, He R, Pan E, et al. Developing fatigue-resistant ferroelectrics using interlayer sliding switching. *Science*. 2024;385(6704):57-62.
23. He R, Zhang B, Wang H, et al. Ultrafast switching dynamics of the ferroelectric order in stacking-engineered ferroelectrics. *Acta Mater*. 2024;262:119416.
24. Wei X-K, Tagantsev AK, Kvasov A, Roleder K, Jia C-L, Setter N. Ferroelectric translational antiphase boundaries in nonpolar materials. *Nat Commun*. 2014;5(1):3031.
25. Yu Z, Fan N, Fu Z, et al. Room-temperature stabilizing strongly competing ferrielectric and antiferroelectric phases in PbZrO3 by strain-mediated phase separation. *Nat Commun*. 2024;15(1):3438.

How to cite this article: Shi Y, Wang R, Zhong Z, et al. Domain and switching dynamics in antiferroelectric $PbZrO_3$: Machine learning molecular dynamics simulation. *MGE Advances*. 2025;e70012. https://doi.org/10.1002/mgea.70012